EEET ECOLOGICAL ENGINEERING & ENVIRONMENTAL TECHNOLOGY

Ecological Engineering & Environmental Technology, 2025, 26(6), 303–320
https://doi.org/10.12912/27197050/204410
ISSN 2719–7050, License CC-BY 4.0

Received: 2025.04.02
Accepted: 2025.04.25
Published: 2025.05.03

Geological and structural study of the cobalt and nickel arsenide deposit of Aghbar (Bou Azzer–El Graâra Inlier, Central Anti-Atlas, Morocco): Implications for mineral exploration

Marieme Jabbour[1*], Said Ilmen[2], Moha Ikenne[1],
Faouziya Haissen[3], Younes Moundi[4], Abdelhak Karfal[4],
Mustapha Souhassou[5], Ismail Bouskri[5], Lhou Maacha[4]

[1] Laboratory of Applied Geology and Geo-Environment (LAGAGE), Department of Geology, Ibn Zohr University, B.P 8106, Dakhla, 80 000 Agadir, Morocco
[2] CAG2M, Polydisciplinary Faculty of Ouarzazate, Ibnou Zohr University, Avenue Moulay Ettahar Ben Abdulkarim, BP. 638, 45000 Ouarzazate, Morocco
[3] Department of Geology, Ben M'sik Faculty of Sciences, Hassan II University, Casablanca, Morocco
[4] MANAGEM Group, Twin Center, Casablanca, Morocco
[5] 2 GBEI Laboratory, Polydisciplinary Faculty of Taroudant, Ibnou Zohr University, Agadir, Morocco
* Corresponding author's e-mail: marieme.jabbour@edu.uiz.ac.ma

ABSTRACT

The Aghbar deposit, located in the central part of the Bou Azzer–El Graâra inlier (Anti-Atlas, Morocco), is a cobalt-arsenic-rich mineralization system hosted mainly in Cryogenian serpentinites and their contact with overlying Ediacaran volcanic and volcano-sedimentary formations. This study presents an integrated geological, structural, petrographic, and geochemical analysis aimed to characterize the mineralization and guiding future exploration efforts. Detailed geological mapping, supported by structural measurements, revealed three principal fault families: E–W to WNW–ESE faults associated with Pan-African phase B1; ENE–WSW reverse faults linked to phase B2; and NE–SW to NNE–SSW faults likely related to Hercynian deformation. These structures play a key role in localizing mineralized quartz-carbonate veins, particularly along serpentinite-volcanic contacts. Petrographic analysis confirmed the presence of multiple lithological units including fresh and carbonated serpentinites, Ediacaran rhyolites and dacites, and Adoudounian andesites and dolomites. The mineral assemblage is dominated by cobalt, nickel, and arsenic-bearing phases such as skutterudite, safflorite, and rammelsbergite, often associated with calcite and quartz gangue. Geochemical results from surface and underground samples showed strong positive correlations among cobalt, nickel, and arsenic, with occasional enrichment in copper. Principal component analysis supported these associations and highlighted key geochemical indicators for exploration. The study concludes that mineralization is structurally controlled and favored by lithological contrasts, particularly brecciated and carbonated zones at serpentinite-volcanic interfaces. These findings contribute to refining the metallogenic model of the Bou Azzer district and offer valuable criteria for targeting future cobalt exploration.

Keywords: Aghbar deposit, Bou Azzer, cobalt mineralization, structural analysis, serpentinite, quartz-carbonate veins, Anti-Atlas.

INTRODUCTION

The mining sector occupies an important place in Morocco's economy. According to statistics from the Ministry of Energy, Mines and Sustainable Development (2017 data), the sector represents 10% of GDP, more than 20% of the value of exports with more than 41.0 billion DH, and provides more than 41,000 direct jobs. Through the building of roads and the stimulation of all other local economic sectors, the sector also aids in the opening up of remote areas. Located at the northwestern edge of the West African Craton, the Anti-Atlas belt has recorded multiple geological events (sedimentary, magmatic, tectonic,…) during the orogenies that have succeeded each other in the region over geological time and in particular, the Eburnian, Pan-African and Hercynian orogenies. Gold, Silver, Cobalt, Copper, Nickel, Barite, Manganese, Molybdenum, Lead, and other metallic elements were concentrated due to the succession of these successive events, producing several mining deposits (Fig. 1). In the Co-Ni district of Bou Azzer, from 1934 to 1987, industrial production took over from artisanal mining. Several companies undertook the exploitation of the Bou Azzer deposit for Co, As, Ni and gold (Au). Exploration was based on a model of Hercynian hydrothermal systems associated with serpentinite massifs. In 1987, when the Company of Tifnoute Tiranimine (CTT), belonging to the MANAGEM Group, resumed its activity and discovered new deposits, it focused on the exploitation of Co. Bou Azzer represents about 8% of the annual world production of this metal (Hawkins, 2006). According to the 2016 report of MANAGEM Group, the annual production isaround 1800 tons metal of Co, 188 t of Ni, 352kg of Au.

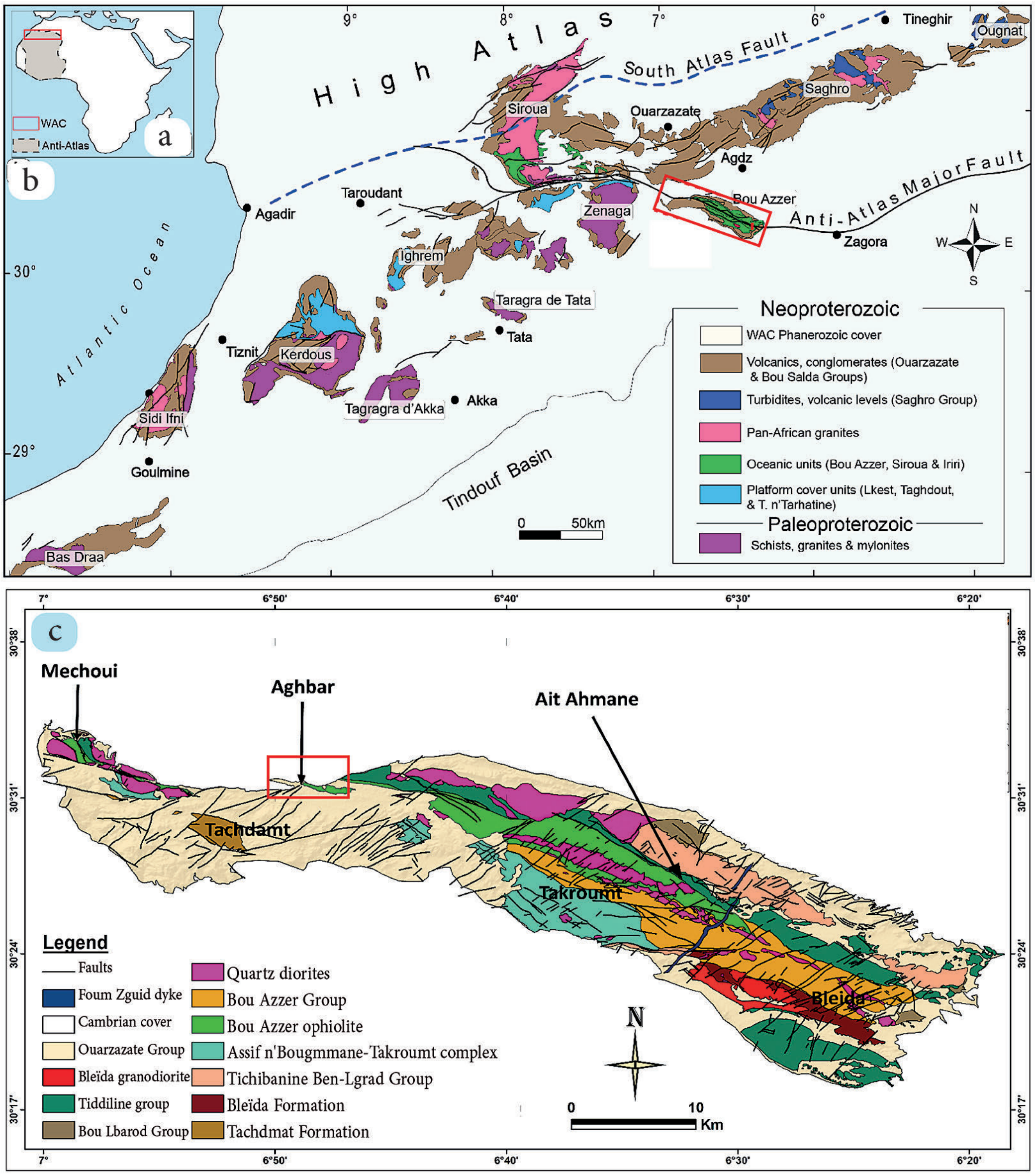

Figure 1. Geological map of the Anti-Atlas belt: (a) Inset showing the location of the Anti-Atlas belt within the framework of the West African Craton, (b) Geological map of the Anti-Atlas (modified from Gasquet et al., 2008), (c) Geological map of the Bou Azzer-El Graara inlier (modified after Yazidi et al., 2007; Admou et al., 2013; Soulaimani et al., 2013a, b; Blein et al., 2013, 2013b, 2013c)

The Aghbar deposit is situated in the central part of the Bou Azzer-El Graâra inlier, a key geological structure within the Central Anti-Atlas of Morocco, renowned for its cobalt-rich mineralization. This area marks a significant lithostratigraphic transition, where Cryogenian serpentinites of the Middle Neoproterozoic are unconformably overlain by Ediacaran volcanic and volcano-sedimentary units. The Bou Azzer-El Graâra mining district, internationally recognized for its Co-Ni-As mineralization, with accessory occurrences of gold and copper, lies within a geodynamically complex framework influenced by multiple orogenic events, notably the Pan-African (B1 and B2 phases) and the Hercynian.

The present study of the Aghbar deposit is part of an integrated geological investigation combining detailed geological mapping at a 1:4000 scale, structural analysis, petrographic characterization, and geochemical profiling. The primary objective is to establish a geological model of the cobaltiferous ore bodies based on litho-structural relationships and host rock facies. Field campaigns enabled the collection of more than forty representative samples across different levels of the deposit, complemented by observations from core drilling (log 19001_AGH/-71), petrographic analyses on thin sections, and chemical analyses performed by atomic absorption spectroscopy (AAS) and inductively coupled plasma atomic emission spectroscopy (ICP-AES).

This work aims to contribute to an understanding of the metallogenic style of the Aghbar deposit by integrating lithological, structural, mineralogical, and geochemical data, in order to support exploration strategies and evaluate both the lateral and vertical potential of the mineralization.

GEOLOGICAL AND STRUCTURAL SETTING

The anti atlas

The Anti-Atlas belt is geologically subdivided into two main domains by the Anti-Atlas Major Fault (AAMF), as defined by Leblanc (1981): a southwestern Paleoproterozoic (Eburnean) domain and a northeastern Neoproterozoic (Pan-African) domain. The southwestern domain exposes Paleoproterozoic siliciclastic sediments and granitoid intrusions (Gasquet et al., 2008), with the oldest units in the western inliers comprising metasedimentary sequences intruded by 2.0 Ga Eburnean granitoids (Aït Malek et al., 1998; Gasquet et al., 2004; Barbey et al., 2004; O'Connor et al., 2010; Blein et al., 2014; Askkour et al., 2023).

In contrast, Paleoproterozoic basement rocks are not observed in the central and eastern Anti-Atlas. However, inherited Paleoproterozoic zircon grains within Neoproterozoic magmatic rocks suggest a buried continuation of these older units beneath the Pan-African domain (Ennih and Liégeois, 2001; Gasquet et al., 2005; Errami et al., 2009; Baidada et al., 2019; El Haibi et al., 2021; Ikenne et al., 2021). Recent geochronological work also confirms the presence of Mesoproterozoic activity, particularly through basic dykes identified in the Zenaga and Bas Drâa inliers (El Bahat et al., 2013; Kouyaté et al., 2013; Söderlund et al., 2013). Ages ranging from ~1380 Ma to ~1655 Ma have been reported. Quartzites from the Igherm inlier yielded a new age of ~1710 Ma, supporting the interpretation of the Taghdout Group as a passive margin sequence formed in the late Paleoproterozoic to early Mesoproterozoic (Ikenne et al., 2017).

The Neoproterozoic evolution of the Anti-Atlas involved a classic Wilson cycle. Rifting and oceanic spreading (Tonian to Cryogenian) were followed by subduction and arc accretion, and eventually post-collisional transtensional evolution (Leblanc and Lancelot, 1980; Leblanc, 1981; Saquaque et al., 1992; Villeneuve and Cornée, 1994; Ennih and Liégeois, 2001; Gasquet et al., 2005, 2008; Hefferan et al., 2012; Blein et al., 2014; Ikenne et al., 2023). During the obduction stage, ophiolitic sequences such as Bou Azzer and Siroua were emplaced, and quartz-diorite intrusions formed around 680–660 Ma (Gasquet et al., 2005). In the post-collisional phase, the Ouarzazate Group (580–540 Ma) was emplaced as a large silicic volcanic province associated with high-K calc-alkaline to shoshonitic magmatism (Thomas et al., 2004; Toummite et al., 2012; Belkacim et al., 2017; Ousbih et al., 2024).

Bou Azzer inlier

A new geological mapping (1/50.000 scale sheet maps of Bou Azzer, Ait Ahmane, Al Gloa, Alougoum and Ait Semgane) has subdivided the Bou-Azzer inlier into various groups (Thomas et al., 2000; Gresse et al., 2000; De Beer et al., 2000) including several Groups. At the base of the sequence lies the Tachdamt–Bleïda formations, which represents a rifted passive margin sequence deposited on the northern flank of the West African Craton during the Tonian–Cryogenian. It comprises metamorphosed stromatolitic limestones, quartzites, mafic sills, lava flows, and felsic volcanic rocks (Leblanc and Billaud, 1978; Mouttaqi and Sagon, 1999). Radiometric dating of crystal-rich and lithic tuffs in the volcanic Tachdamt Formation yields an age of ~883 Ma (Bouougri et al., 2020). These sediments are laterally equivalent to the Taghdout Group in the western Anti-Atlas (Clauer, 1974; Leblanc, 1981; Hassenforder, 1987; Bouougri and Saquaque, 2004), with evidence from the Igherm window (Ikenne et al., 2017) and Zenaga (Aït Lahna et al., 2016) suggesting that some mafic intrusives may be as old as 1.7–1.6 Ga.

Stratigraphically above is the Tazegzaout–Assif n'Bougmmane Group, formerly considered Paleoproterozoic (Leblanc, 1981), but now constrained to ~750 Ma based on zircon U–Pb ages of 755 ± 9 Ma and 745 ± 5 Ma from orthogneiss protoliths, and 695 ± 7 Ma from the Oumlil leucogranodiorite (D'Lemos et al., 2006; Chèvremont et al., 2013; Blein et al., 2014a; Hefferan et al., 2014). This unit consists of orthogneiss, metagabbro, amphibolites, schists, and pegmatite. The Bougmmane complex within this group includes 750–730 Ma felsic–mafic orthogneisses intruded by tonalites and hornblende gabbros dated between 710–690 Ma (Triantafyllou et al., 2018, 2020), indicating early Cryogenian magmatism linked to oceanic arc development. The Tichibanine–Ben Lgrad Group, located in the northern part of the inlier, comprises volcanic sequences ranging from basaltic to rhyolitic composition, with radiometric ages of ~761–762 Ma (Samson et al., 2004). These rocks are interpreted as components of an intra-oceanic volcanic arc formed during rifting (Admou et al., 2013), later involved in arc accretion events.

The central portion of the inlier is dominated by the Bou Azzer–El Graara Group, which includes a well-preserved ophiolitic complex. This suite has been variably interpreted as either a back-arc (Bodinier et al., 1984; Triantafyllou et al., 2018) or fore-arc system (Naidoo et al., 1991), characterized by basaltic lavas displaying supra-subduction zone affinities and positive εNd values (6.3–8.1), consistent with juvenile mantle sources (Naidoo et al., 1991; Ikenne et al., 2005; Ahmed et al., 2009; Walsh et al., 2012; Hefferan et al., 2014; Arenas et al., 2020; Hodel et al., 2020). Following ophiolite emplacement, erosion of uplifted terranes led to the development of Neoproterozoic intracontinental basins such as Bou Salda, Anezi, Tiddiline, and Dadès (Gasquet et al., 2008; Abati et al., 2010; Álvaro et al., 2014b).

Unconformably overlying the ophiolite is the Tiddiline Group, exceeding 1000 meters in thickness and composed of polymict conglomerates, feldspathic sandstones, shales, volcanic interbeds, and glaciomarine tillites. The unit records sedimentation in a shallow marine to glaciomarine environment, with glacial dropstones and diamictite intercalations pointing to ice-rafted debris and fluctuating glacial conditions (Leblanc and Lancelot, 1980; Deynoux et al., 2006; Letsch et al., 2018). Hypabyssal intrusions, including microdiorites and spilites, are coeval with the Tiddiline sedimentation. Structurally, the Tiddiline Group is fragmented by sinistral strike-slip faults, forming two WNW corridors with continuous outcrops in the north and isolated patches in the south near Bou Azzer, Tachdamt, and Trifya. It is now considered the basal unit of the revised Ouarzazate Supergroup (Thomas et al., 2004).

Post-collisional processes are recorded by the Ouarzazate Group (560–543 Ma), which caps the Bou Azzer succession and consists of high-K calc-alkaline to shoshonitic volcanic and volcaniclastic rocks, along with minor basalt, rhyolite, ignimbrites, lapilli tuffs, and epiclastic sediments (Thomas et al., 2004; Toummite et al., 2012; Belkacim et al., 2017; Ousbih et al., 2024). Four subgroups (Tiouin, Bouljama, Tafrant, and Achkoukchi) are identified in the Sirwa inlier based on geometry, lithology, and stratigraphic relationships (Thomas et al., 2000a). Isotopic data (εNd > 0; low 87Sr/86Sr) confirm derivation from juvenile mantle sources (Toummite et al., 2013).

A key metallogenic feature is the Ambed Formation, also known as the "carapace d'Ambed," a silica–carbonate crust developed through meteoric and hydrothermal alteration of serpentinite massifs (Leblanc, 1981). It contains siliciclastic and carbonate interbeds and iron- and sulfide-bearing horizons indicative of hydrothermal processes. The Ambed unit is structurally deformed by Pan-African and Hercynian faulting and serves as a critical mineralizing horizon due to its permeability and proximity to major shear zones (Leblanc and Lancelot, 1980; Maacha et al., 2015; Tourneur et al., 2023). It is now widely used in exploration targeting surface indicators of Co–Ni mineralization, with several studies confirming metal enrichment via leaching from underlying serpentinites (Leblanc, 1975; Maacha, 2013; Bouabdellah et al., 2016; Hodel et al., 2017; Hajjar et al., 2021).

MATERIALS AND METHODS

This study integrates field investigations, petrographic and structural analysis, and laboratory geochemical techniques to characterize the lithological, mineralogical, and structural controls on the Aghbar Co–Ni–As deposit. The methodological workflow combines geological mapping, outcrop logging, sampling, thin section analysis, structural interpretation, and geochemical assays.

Fieldwork and sample selection

Fieldwork was conducted within the Bou Azzer mining district, with a focus on the Aghbar deposit. Geological and structural mapping was performed at a scale of 1:4000 across the main mineralized zone. Lithological boundaries, fault traces, shear zones, and quartz-carbonate veins were systematically recorded. Structural data collection included 83 orientation measurements of faults and mineralized veins, using a Brunton compass, measuring tape, and handheld GPS for spatial reference.

Representative sampling was carried out across surface outcrops, underground galleries, and drill cores (notably borehole 19001_AGH/-71). A total of 22 rock samples were selected based on mineralization style, lithological diversity, and spatial coverage. Sampling aimed to capture the vertical and lateral variability of the host rocks and ore zones, across five main depth intervals ranging from surface to –405 meters. Samples included serpentinites (altered and carbonated), rhyolites, andesites, dolomites, and vein systems containing visible mineralization.

Petrographic analysis

Collected samples were first described macroscopically for mineralogy, texture, and alteration features. Polished thin sections were prepared at the Reminex Research Center in Marrakech, following standard procedures. Microscopic examination was conducted at the Faculty of Sciences, Agadir (Department of Geology), using an Olympus BX41 optical microscope equipped with transmitted and reflected light capabilities, and a Sony TOUPCAM camera for digital imaging. Observations focused on ore mineral associations, replacement textures, gangue composition, and paragenetic relationships.

Structural analysis

Structural data were processed and interpreted using stereographic projection and rose diagram analysis with the Win-Tensor software. Fault families were classified based on orientation and kinematics, and their spatial correlation with mineralized structures was assessed. Geological cross-sections and lithological logs were prepared to interpret fault displacement, ore geometry, and vertical evolution of facies.

Geochemical sampling

Geochemical sampling was designed to capture variations in metal content across different lithologies and depths. A total of 40 representative samples were analyzed for major and trace element concentrations. Sample powders were prepared by crushing and homogenizing fresh chips using an agate mortar. Analytical work was performed at the Reminex Research Center (Marrakech) using atomic absorption spectrometry (AAS) and Inductively Coupled Plasma Atomic Emission Spectrometry (ICP-AES).

For ICP-AES analysis, sample powders were digested using the Water Regal method. A mass of 0.5 g of powdered sample was weighed and digested in 10 mL of 68% nitric acid and 15 mL of 30% hydrochloric acid. The solution was placed on a 150 °C hot plate and evaporated to dryness. The dry residue was redissolved with 60 mL of 38% hydrochloric acid and heated again at 200 °C for 15 minutes. The final solution was diluted and transferred into a 200 mL volumetric flask.

Major elements were determined by ICP-AES using radial plasma reading, and calibrated against four natural standard concentrations (2.5, 5, 10, and 20 ppm). Trace elements were analyzed using axial plasma reading, providing higher sensitivity for low-concentration elements.

Data processing and visualization

Geological maps, cross-sections, and stratigraphic columns were digitized and finalized using AutoCAD and Covadis software.

Geochemical data were processed with Excel and statistical analysis tools. Principal component analysis (PCA) was performed to identify element associations and guide interpretation of ore-related geochemical signatures.

RESULTS

Field and petrographic observations of the Aghbar deposit

The Aghbar deposit is located in the western-central part of the Bou Azzer inlier and represents one of the most significant Co–Ni–As–Fe occurrences within the Bou Azzer mining district. The mineralization is spatially associated with a diapiric serpentinite body intruding into the Ediacaran volcanic and volcano-sedimentary sequences of the PIII unit. This serpentinite, interpreted as a remnant of Neoproterozoic oceanic lithosphere obducted during the Pan-African orogeny, forms the core of the Aghbar structure and plays a critical role in controlling the geometry and distribution of the ore bodies (Gervilla et al., 2012, Maacha 2013) (Fig. 2).

Geologically, the deposit is characterized by a structural and lithological contact between the serpentinite dome and its surrounding volcanic cover, composed mainly of ignimbrites, rhyolitic tuffs, and brecciated pyroclastic rocks. The contact is tectonized and locally brecciated, providing pathways for fluid circulation and metasomatic replacement. The mineralized zone displays a concave-down geometry and consists of a complex shell surrounding the serpentinite, occasionally deformed into subvertical, flame-shaped ore shoots (Leblanc and Billaud, 1982; Gervilla et al., 2012). The most economically significant mineralized body is a lode-shaped structure along the southern border of the serpentinite, measuring approximately 600 meters in length and 2 to 10 meters in thickness, exploited to depths of over 400 meters.

The host serpentinites are strongly altered and exhibit widespread carbonatization, talcization, and serpentinization. Textural remnants of

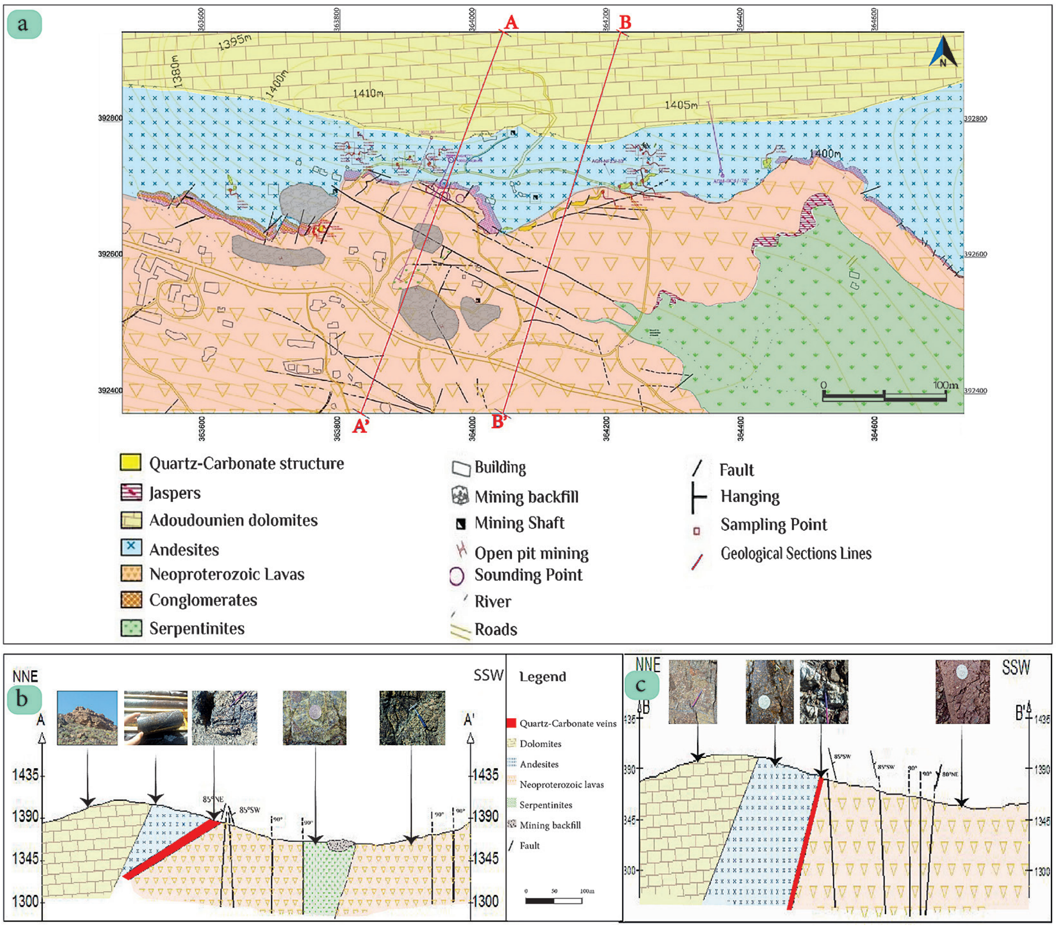

Figure 2. (a) Geological map of the Aghbar ore deposit, (b;c) Geological cross-sections

olivine and chromite are often preserved, with chromite frequently found as inclusions in arsenide minerals, indicating a genetic link between the ultramafic host and the ore assemblages (Gervilla et al., 2012). In certain areas, especially to the east of the dome, a silica–carbonate alteration crust is developed, known as the Ambed Formation, which reflects hydrothermal overprinting and near-surface weathering of ophiolitic material (Leblanc and Billaud, 1982) (Fig. 2).

The Aghbar deposit, located in the central-western part of the Bou Azzer inlier, represents one of the most significant Co–Ni–As–Fe mineralized systems in the district. The ore is spatially controlled by a diapiric serpentinite body that intrudes the Ediacaran volcanic and volcano-sedimentary rocks of the PIII unit. This serpentinite, considered a remnant of Neoproterozoic oceanic lithosphere obducted during the Pan-African orogeny, forms the structural core of the deposit and plays a key role in the localization and geometry of mineralized bodies (Gervilla et al., 2012; Maacha, 2013).

The contact between the serpentinite and the surrounding Ediacaran ignimbrites, tuffs, and breccias is structurally complex, frequently brecciated and mineralized, forming a concave shell-like mineralized zone occasionally folded into subvertical, flame-shaped ore shoots (Leblanc & Billaud, 1982). The main economic body is located along the southern edge of the serpentinite and reaches over 600 m in length and up to 10 m thick, extending to depths beyond 400 m (Fig.3).

The serpentinites are strongly altered, exhibiting widespread serpentinization, carbonatization, and talcization. Petrographic analysis distinguishes two main types: massive and carbonated serpentinites. These rocks host arsenide mineralization, with chromite remnants frequently enclosed in arsenide phases, indicating metasomatic replacement during mineralization (Gervilla et al., 2012).

The Ediacaran volcanic rocks (PIII), mainly rhyolites and dacites, are also affected by hydrothermal alteration. Adoudounian andesites and dolomites overlie the PIII unit and locally host quartz-carbonate veins, often brecciated or stockwork-type (Fig. 3).

Structural framework

The structural framework of the Aghbar deposit is shaped by a complex tectonic history inherited from multiple phases of the Pan-African orogeny and subsequent tectonic reactivations. The Bou Azzer inlier, where Aghbar is located, has recorded more than twenty major fault systems, among which three structural networks play a fundamental role in controlling the localization and geometry of the mineralization. The first is the Filon II–Aghbar North fault system, composed of inherited structures that influenced the development of the northern Infracambrian basins along the northern edge of a Precambrian horst. This system is dominated by faults trending approximately N95°, with secondary oblique structures oriented around N80° responsible for the tectonic uplift of serpentinite slices and vertical displacements of the cover units. The second major structural domain lies between Bou Azzer East and Aghbar, and includes a series of faults with varying orientations from N35° to N110°, exhibiting predominantly sinistral strike-slip movement. These faults segment the basement into blocks with a cumulative displacement exceeding six kilometers and have experienced complex kinematic histories, including vertical, thrust, and normal components likely associated with the Variscan and Atlasic compressional events. The third key structure is the South Aghbar fault, trending nearly east–west with a steep southward dip of about 70°, which appears to have controlled the transtensive basins hosting the Neoproterozoic III volcanic and volcano-sedimentary formations. This fault also marks a lithological boundary between the dioritic massif and the serpentinite to the east.

Structural mapping of the deposit area reveals two dominant fault families: one trending northeast–southwest, and the other northwest–southeast, the latter being more extensively developed. These fault sets are composed of strike-slip structures, both dextral and sinistral, and host a dense network of quartz–carbonate veins, most of which are mineralized. They are likely related to the Pan-African B2 phase, which reactivated earlier discontinuities formed during the B1 event, and may also include later reactivations during the Variscan cycle. Fault measurements from the field show variable orientations and dips, with dominant trends in the E–W, NW–SE, and NE–SW directions. Stereographic analysis identifies four main fault families, with the ENE–WSW and WNW–ESE orientations being the most prominent, followed by NE–SW and NW–SE trends. Most faults dip toward the north–northeast and the southwest (Fig. 4A).

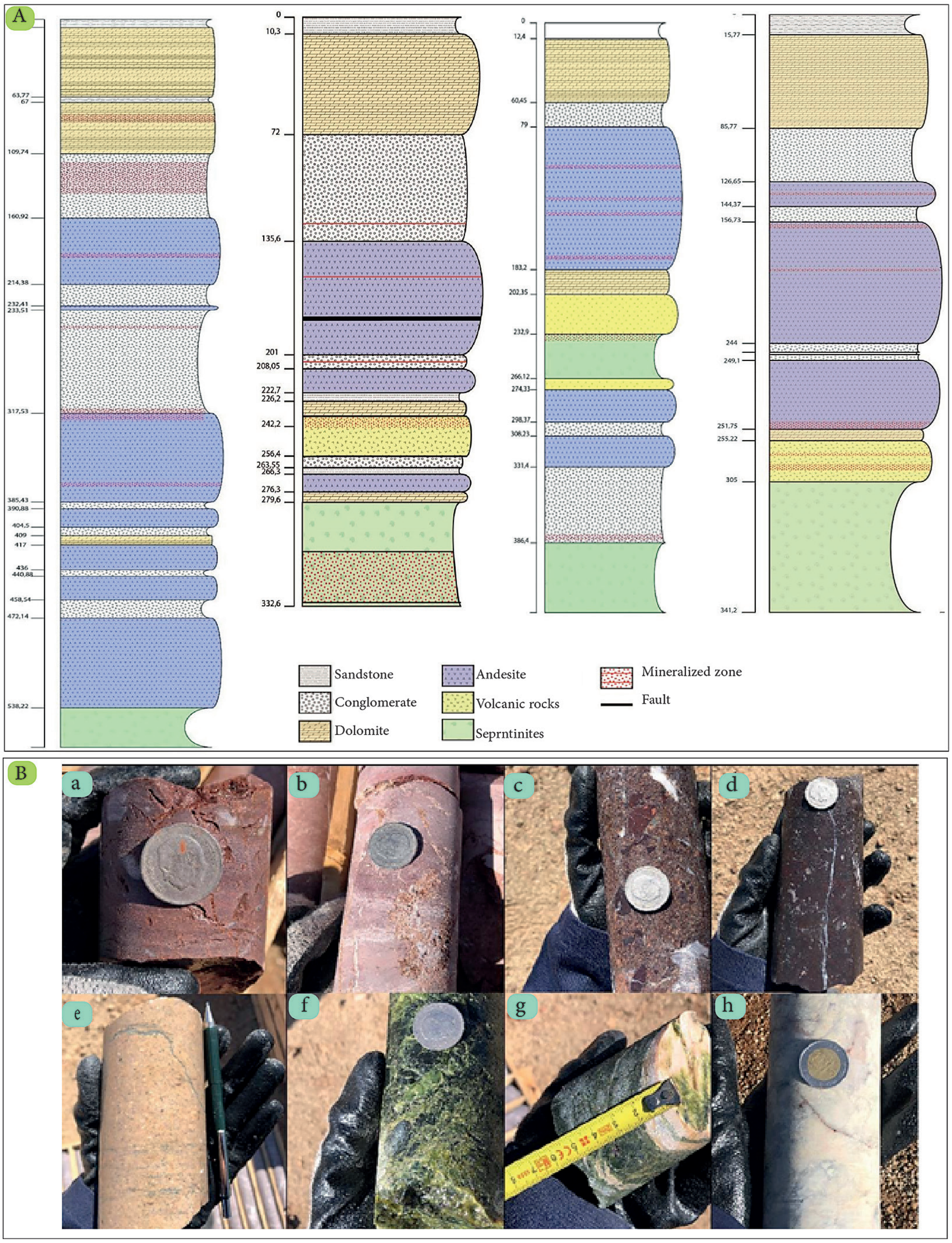

Figure 3. (A) Stratigraphic log of the drill cores in the deposit; (B) Photographs of drill cores: (a) Sandstone, (b) Dolomite, (c) Conglomerate, (d) Andesite, (e) Dacite, (f, g) Serpentinite, (h) Quartz-carbonate vein

The The structural framework of the Aghbar deposit reflects multiple tectonic events from the Pan-African to Hercynian orogenies. Field mapping and structural measurements (>100) highlight three main fault families (Fig. 4):

- E–W to WNW–ESE faults: Interpreted as Pan-African B1 inherited structures, related to ophiolite obduction.
- ENE–WSW faults: Reverse faults attributed to the B2 phase, often brecciated and mineralized.
- NE–SW to NNE–SSW faults: Less dominant but locally important, associated with Hercynian deformation.

Strike-slip faults, frequently observed within dolomitic units, are predominantly dextral, though

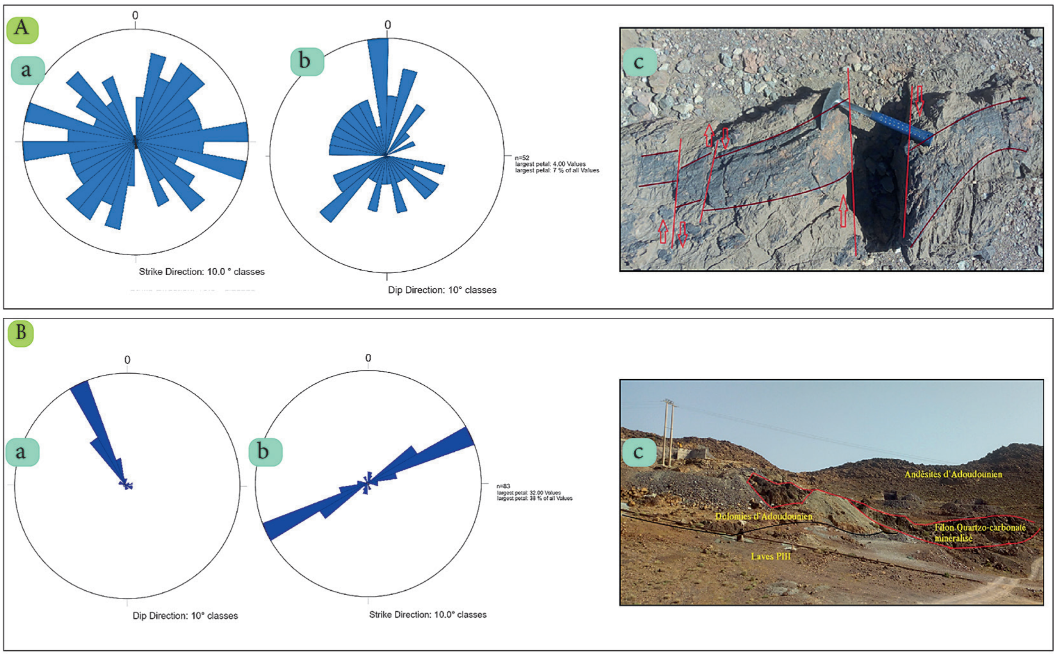

Figure 4. (A) Structural map of the Aghbar deposit, Bou Azzer–El Graâra, Central Anti-Atlas; (B) Stereographic presentation of faults: (a) Rose diagram of fault orientations, (b) Rose diagram of dip directions, (c) Dextral strike-slip fault within the Adoudounian dolomites; (C): Stereographic presentation of mineralized veins: (a) Rose diagram of vein orientations, (b) Rose diagram of dip directions, (c) Mineralized quartz–carbonate vein

conjugate patterns occasionally occur. These structures play an essential role in the mechanical preparation of the host rocks and the opening of fluid pathways. The majority of mineralized structures in the area are veins and veinlets filled with quartz and silica, often enriched in cobalt and gold. Statistical analysis of over eighty quartz–carbonate veins indicates a dominant northeast–southwest trend with dips to the northwest. These structures served as conduits for hydrothermal fluids, facilitating metal transport and precipitation, and remain key exploration targets for ongoing cobalt and arsenic mineral exploration (Fig. 4).

Co-Ni-Cu mineralization characteristics

Mineralization occurs in two main styles (Fig. 5): (i) quartz-carbonate vein-type mineralization, often structurally controlled, and (ii) replacement-type mineralization within serpentinites. Thin section analysis (n > 40) from both surface and underground levels (e.g., drill hole 19001_AGH/-71) reveals a polyphase ore system characterized by three paragenetic stages (Gervilla et al., 2012):

1. Nickel-Rich Arsenide Stage: Early vein-type ores featuring nickeline (NiAs), rammelsbergite ($NiAs_2$), and Ni-rich skutterudite [$(Co,Ni,Fe)As_3$]. Zoning and exsolution textures indicate evolving hydrothermal fluids. Chromite inclusions are common.
2. Cobalt-Iron Arsenide Stage: The dominant phase, with cobaltite- and safflorite-group minerals [$(Co,Ni)AsS$ and $(Fe,Co)As_2$], as well as arsenopyrite. These minerals appear idiomorphic to granular and are commonly arranged along shear planes and faults.
3. Copper-Rich Sulfide Stage: A late-stage overprint characterized by bornite, chalcopyrite, tennantite, and wittichenite. These minerals replace earlier arsenides or fill fractures, associated with quartz, barite, and iron oxides.

The mineralization is closely associated with hydrothermal calcite and pink dolomite, which constitute the main gangue minerals, while quartz is present only in trace amounts. Calcite is the dominant carbonate phase. Three distinct generations of carbonates have been identified: a generation of coarse-grained crystals, a second composed of fine-grained, homogeneous crystals, and a late-stage generation that fills veinlets crosscutting the earlier assemblages. The cobalt mineralization is most often associated with the coarse-grained carbonate generation, suggesting a spatial and temporal link between mineral precipitation and hydrothermal carbonate formation

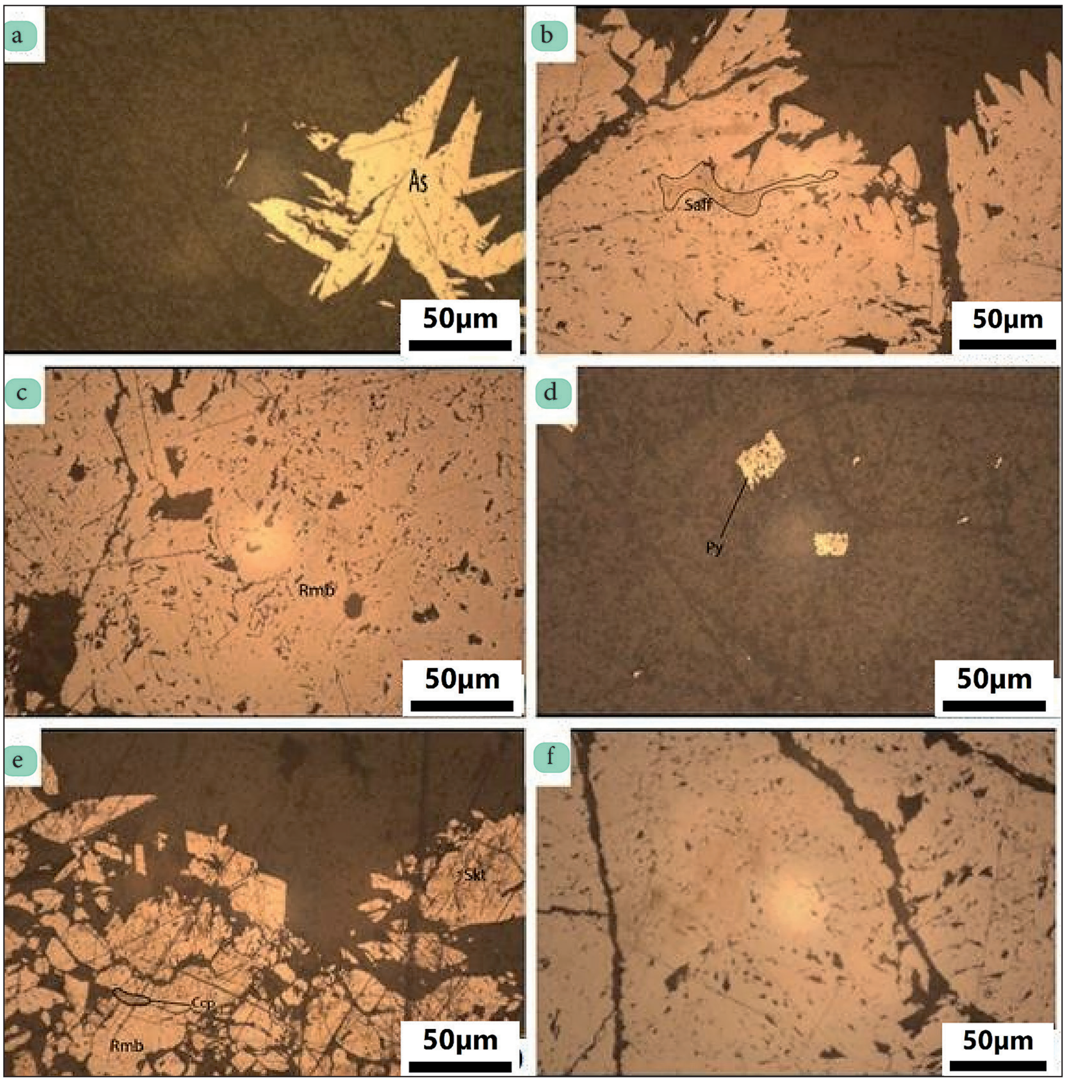

Figure 5. Photomicrographs of cobalt mineralization: (a) Arsenopyrite, (b) Safflorite associated with rammelsbergite, (c) Rammelsbergite, (d) Pyrite, (e) Chalcopyrite, (f) Skutterudite surrounded by rammelsbergite.

(Fig. 6). These carbonates are interpreted as secondary phases, precipitated in response to hydrothermal fluid circulation. In some samples, barite crystals are also present, easily distinguished by their well-developed cleavage and tear-shaped terminations (Fig. 6). In deeper levels of the deposit, barite occasionally appears in association with hematitized pyrite pseudomorphs, identifiable by their brownish hue under reflected light. The cobaltiferous mineralization at Aghbar is observed microscopically in two main modes: either as disseminated grains with uniform crystal habit or as dense, massive aggregates embedded in the carbonate matrix (Fig. 5).

Geochemical analyses of over 40 samples (AAS and ICP-AES) (Table 1) indicate a strong positive correlation between Co, Ni, and As, confirming their genetic association. Co values range from 300 to over 5000 ppm, with high R^2 values for Co–Ni (0.85), Co–As (0.88), and Ni–As (0.81). A secondary association includes Cu, Mo, Au, and Ag, with copper occurring in late-stage veins. PCA analysis confirms two geochemical populations: an early Co-Ni-As group and a later Cu-Mo-Au-Ag association (Fig. 7) (Tables 2, 3).

DISCUSSION

The The Aghbar deposit represents a particularly illustrative example of the Co–Ni–As–Fe metallogenic system in the Bou Azzer mining district, and its study contributes significantly to the understanding of mineralization processes associated with ophiolitic suites in a Pan-African structural context. The results obtained in this work

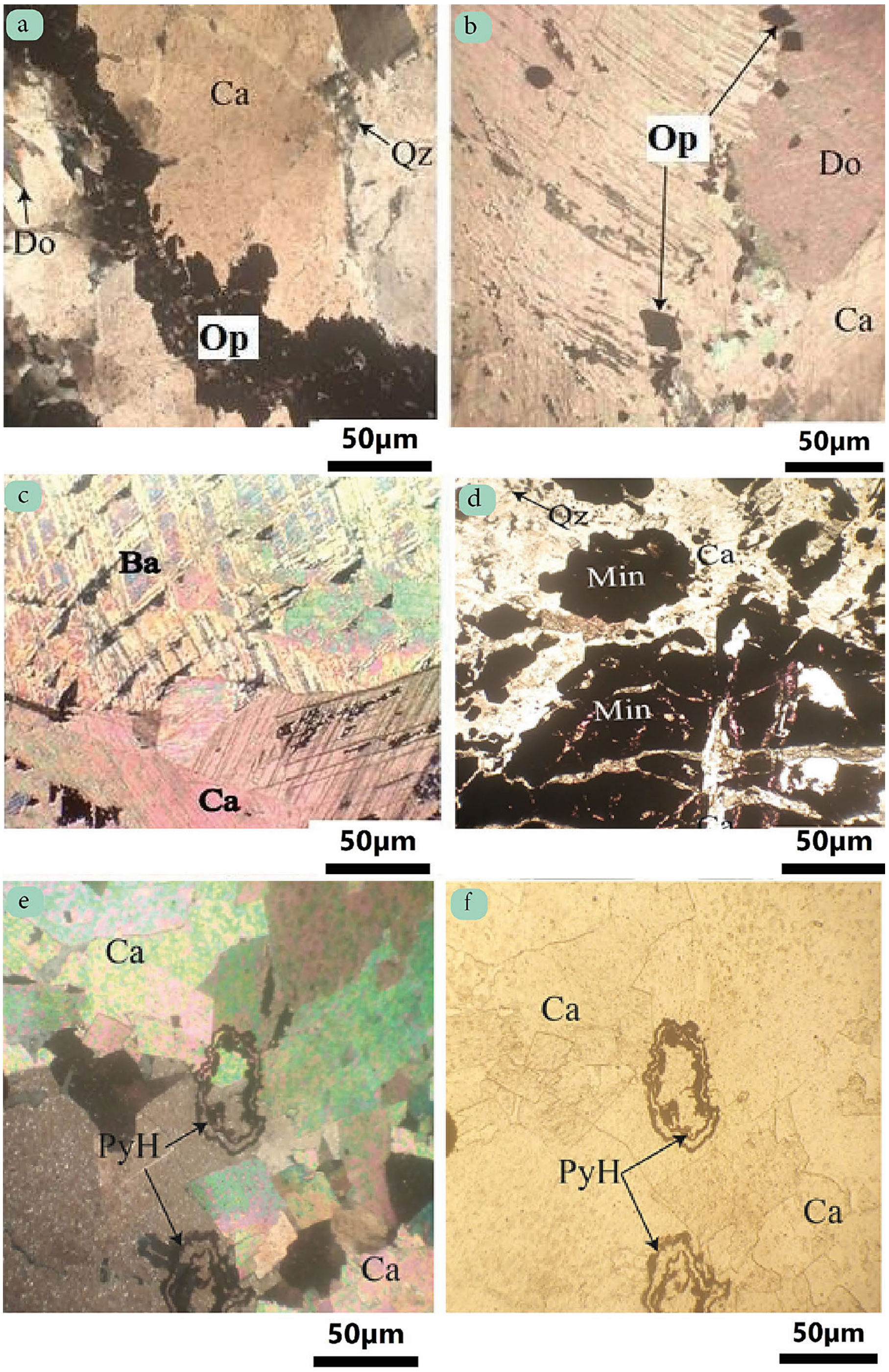

Figure 6. Microscope photographs: (a) Quartz–carbonate gangue with massive veinlet of cobalt arsenides collected at –45 m depth (Min: Cobalt mineralization; Qz: Quartz; Ca: Calcite; Do: Dolomite), (b) Carbonate gangue with disseminated cobalt arsenides collected at –145 m depth (Min: Cobalt mineralization; Ca: Calcite; Do: Dolomite), (c) Carbonate gangue containing barite minerals collected at –325 m depth (Ba: Barite; Ca: Calcite), (d) Massive cobalt arsenide mineralization crosscut by calcite veinlets, collected at –405 m depth (Min: Cobalt mineralization; Ca: Calcite; Qz: Quartz), (c, d) Carbonate gangue with hematitized pyrite showing a colloform texture, collected at –405 m depth (Ca: Calcite; PyH: Hematitized pyrite)

confirm and refine earlier interpretations proposed by Maacha (2013), Gervilla et al. (2012), and Tourneur (2019), among others.

From a litho-structural perspective, the spatial association of mineralization with the serpentinite dome and its bounding faults underscores the importance of both lithological and structural controls. The main ore bodies are localized at the contact zones between the serpentinite core and the overlying Ediacaran volcanic units

Table 1. Geochemical analysis report performed by ICP-AES

	AGH 01	AGH 02	AGH 03	AGH 04	AGH 05	AGH 06	AGH 07	AGH 08	AGH 09	AGH 10	AGH 11	AGH 12	AGH 13	AGH 14	AGH 15	AGH 16	AGH 17	AGH 18	AGH 19	AGH 20	AGH 21	AGH 22	AGH 20 BIS
SiO2	4,33	53,84	60,75	31,15	9,96	6,45	55,13	62,45	39,2	17,07	58,1	58,68	1,65	25,57	0,1	26,24	0,1	0,1	0,1	0,1	31,91	0,1	0,1
Al2O3	0,43	11,16	15,52	0,71	0,48	1,42	12,72	17,62	1,62	3,99	14,99	17,26	0,62	3,16	0,1	0,42	0,11	0,16	0,34	0,36	18,1	0,23	0,48
Fe2O3	0,99	7,31	8,8	4,44	2,87	3,88	5,94	1,94	3,14	2,29	2,19	2,51	3,67	4,16	1,16	0,72	1,78	6,7	0,7	13,83	10,5	0,7	15,9
CaO	33,11	2,7	1,51	14,34	27,95	4,38	0,2	0,63	7,93	24,24	5,28	5,03	33,87	22,33	65,36	41,88	27,62	54,69	63,67	18,22	1,25	56,52	20,98
MgO	19,89	3,01	1,93	27,15	20,07	6,84	23,31	3,44	6,91	17,15	6,24	4,83	21,86	15,75	0,1	1,63	18,66	0,47	1,77	1,74	26,16	0,97	1,56
K2O	0,38	6,68	8,36	0,2	0,2	0,19	0,21	9,87	0,64	2,3	9,98	8,56	0,36	1,02	0,2	0,23	0,19	0,19	0,19	0,18	0,18	0,19	0,19
MnO	0,48	0,09	0,12	0,49	1,57	0,24	0,07	0,01	0,22	0,64	0,15	0,13	1,07	0,88	0,63	0,8	0,53	0,51	0,65	0,22	0,17	0,65	0,27
TiO2	0,01	0,59	0,59	0,01	0,01	0,01	0,41	1,09	0,05	0,22	1,22	1,3	0,02	0,14	0,01	0,01	0,01	0,01	0,01	0,01	3,33	0,01	0,01
P2O5	0,02	0,12	0,1	0,01	0,01	0,01	0,05	0,27	0,01	0,06	0,41	0,36	0,01	0,02	0,01	0,01	0,01	0,01	0,01	0,01	0,57	0,01	0,01
As	48	38	77	391	2578	391622	3724	1000	200882	2234	502	134	559	30797	6744	211	7242	50918	1533	336984	2917	258	339767
B	14	47	55	39	5	5	13	144	5	19	22	74	9	12	5	5	5	7	5	20	19	10	13
Ba	61	262	353	3	8	19	27	872	53	130	1095	665	14	23	41	18	131	36	16	13	10	9	12
Be	0,2	0,2	0,2	0,2	0,2	0,9	0,8	0,2	0,3	0,5	0,2	0,2	0,8	0,4	0,8	8,7	1,1	0,7	1,1	1,3	0,2	0,7	1,1
Bi	35	20	20	20	24	163	20	20	78	23	20	20	20	40	20	20	30	34	34	113	20	20	133
Cd	2	2	2	2	16	10084	118	30	4768	41	9	3	12	737	157	6	224	2218	39	9770	75	7	9540
Co	8	46	17	25	222	137133	1580	360	50423	663	78	25	77	7606	227	8	2156	7694	78	29618	338	19	31534
Cr	47	57	104	1184	1693	212	73	60	137	45	111	62	32	97	27	1524	57	39	457	1179	293	41	952
Cu	679	60	104	3520	284	1325	68	534	90	95	89	67	195	2300	93	248	811	1668	617	1363	1478	49	1447
Ge	14	10	12	10	10	10	17	10	10	10	20	10	10	10	10	10	10	10	10	10	18	10	10
Li	15	41	20	39	20	34	189	39	28	22	51	63	15	23	15	20	15	15	15	15	288	15	18
Mo	8	8	8	8	8	7717	104	11	3862	283	12	8	8	1017	11	111	81	119	756	46	8	8	48
Nb	1	127	95	1	1	62	14	46	2	1	5	34	1	1	1	1	1	1	1	1	87	1	1
Ni	20	33	24	782	399	11064	1228	95	7660	125	97	65	30	556	29	140	146	352	88	1516	904	22	1393
Pb	246	26	39	26	26	78	26	60	45	31	26	26	83	452	26	77	27	140	26	33	26	26	36
S	0,0564	0,0576	0,0415	0,32	0,0596	0,84	0,0549	0,039	0,5	0,0647	0,0408	0,0393	0,0588	0,36	0,16	0,0547	0,0736	0,5	0,15	0,31	0,18	0,0496	0,31
Se	40	40	40	40	40	569	40	40	57	40	40	40	40	40	40	40	40	40	40	40	40	40	40
Sn	33	20	28	20	20	20	20	20	20	20	20	20	20	20	20	20	20	20	20	20	20	20	20
Sr	87	27	25	45	62	6	5	21	16	23	34	38	27	31	244	252	41	190	231	107	10	170	106
Y	3	83	61	2	13	5	18	11	12	55	19	20	94	30	76	36	59	57	39	22	7	28	20
Zn	256	49	89	109	94	287	118	80	169	58	79	124	147	954	171	139	121	86	82	144	131	40	116
Sb	32	32	32	32	32	32	32	32	32	32	32	32	32	32	32	32	32	32	32	32	32	32	32
W	23	23	23	23	23	23	23	23	23	23	23	23	23	23	23	23	23	23	23	23	23	23	23
PF	44,15	4,93	3,41	23,43	38,69	20,88	8,88	3,12	15,56	35,2	5,45	5,88	44,7	26,22	41,35	30,76	44,05	27,77	41,82	9,68	10,92	43,03	9,41

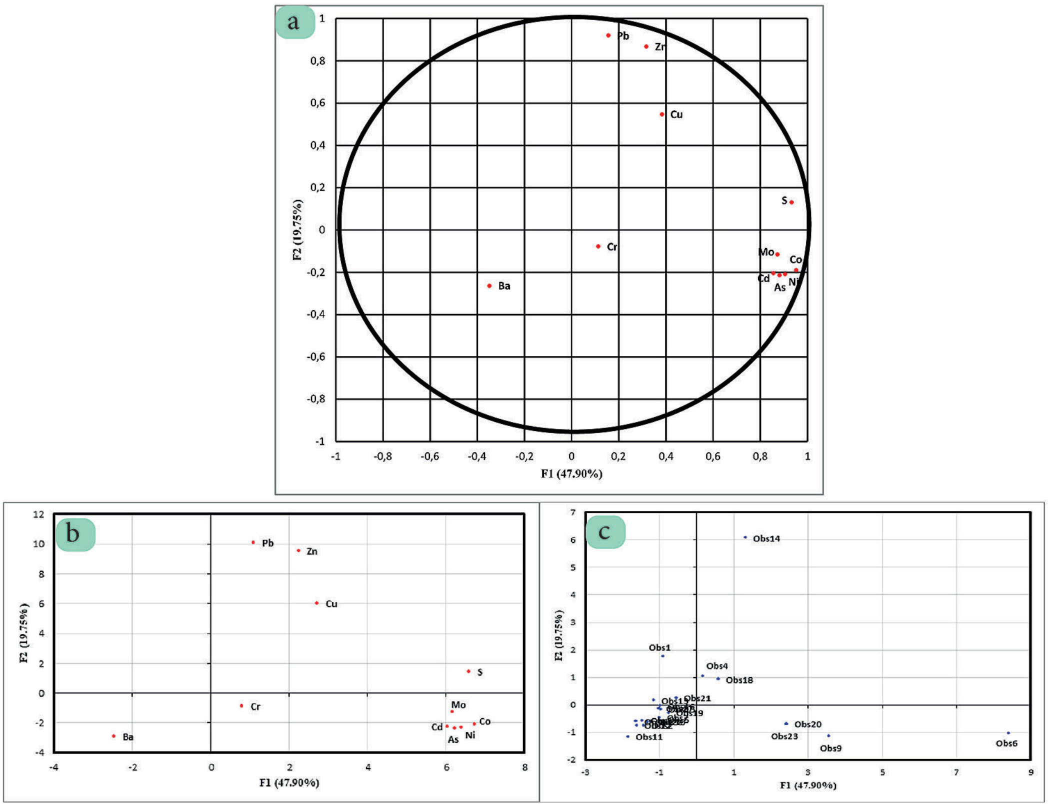

Figure 7. (a) Principal component analysis (PCA) of chemical elements, (b, c) Principal component analysis (PCA) of Aghbar samples

(PIII), where brecciation, fracturing, and hydrothermal alteration are most intense. This observation aligns with Maacha’s (2013) categorization of Aghbar-type mineralization, controlled by diapiric ascent of serpentinites and syn-mineral fracturing. The geometry of the mineralized envelope, with its concave morphology and subvertical ore shoots, reflects intense post-emplacement deformation. The NE–SW to ENE–WSW trending veins, with NW dips, appear to be the main metallotects. These structures correspond to B2 phase faults and are often associated with fault breccias and replacement textures, consistent with the observations of Tourneur (2019), who emphasized the role of transtensive fault systems in guiding mineralizing fluids.

Petrographic and mineralogical studies indicate a polyphase mineralizing system. The paragenetic evolution begins with a high-temperature Ni-rich arsenide stage, featuring nickeline, rammelsbergite, and Ni-rich skutterudite. The paragenetic evolution of the deposit is

Table 2. Statistical summary of geochemical data

Variable	Minimum	Maximum	Mean	Standard deviation
As	38	391622	60050.435	124947.11
Ba	3	1095	168.304	300.75
Cd	2	10084	1646.174	3398.661
Co	8	137133	11736.304	30283.898
Cr	27	1693	368.826	529.91
Cu	49	3520	747.13	892.902
Mo	8	7717	619.565	1749.98
Ni	20	11064	1163.826	2678.138
Pb	26	452	69.87	97.473
Zn	40	954	158.391	183.128
S	0,04	0.84	0.19	0.21

Table 3. Correlation matrix of chemical elements

Variables	As	Ba	Cd	Co	Cr	Cu	Mo	Ni	Pb	Zn	S
As	1	-0.242	0.996	0.829	0.230	0.255	0.627	0.719	-0.043	0.105	0.739
Ba	-0.242	1	-0.245	-0.190	-0.298	-0.312	-0.166	-0.197	-0.161	-0.190	-0.351
Cd	0.996	-0.245	1	0.792	0.245	0.276	0.571	0.667	-0.043	0.088	0.724
Co	0.829	-0.190	0.792	1	0.009	0.174	0.942	0.946	0.014	0.177	0.841
Cr	0.230	-0.298	0.245	0.009	1	0.300	-0.114	-0.033	-0.177	-0.109	0.038
Cu	0.255	-0.312	0.276	0.174	0.300	1	0.095	0.112	0.368	0.408	0.530
Mo	0.627	-0.166	0.571	0.942	-0.114	0.095	1	0.964	0.082	0.246	0.799
Ni	0.719	-0.197	0.667	0.946	-0.033	0.112	0.964	1	-0.023	0.153	0.818
Pb	-0.043	-0.161	-0.043	0.014	-0.177	0.368	0.082	-0.023	1	0.898	0.226
Zn	0.105	-0.190	0.088	0.177	-0.109	0.408	0.246	0.153	0.898	1	0.339
S	0.739	-0.351	0.724	0.841	0.038	0.530	0.799	0.818	0.226	0.339	1

polyphased, with three main stages as defined by Gervilla et al. (2012):

- Ni-rich Arsenide Stage: The earliest phase features vein-hosted minerals such as nickeline, rammelsbergite, and Ni-rich skutterudite. These minerals crystallized under high-temperature conditions (~650–625 °C) with increasing arsenic fugacity. Oscillatory zoning and exsolution textures indicate re-equilibration with evolving fluids.
- Co–Fe Arsenide Stage: Dominant in terms of volume, this stage includes safflorite, cobaltite–gersdorffite, and löllingite, typically hosted in altered serpentinites. The lower temperature range (~500–400 °C) and metasomatic textures suggest significant fluid–rock interaction, particularly along fault zones and brecciated contacts.
- Late Cu-bearing Sulfide Stage: Characterized by bornite, chalcopyrite, tennantite, and molybdenite, this overprint replaces earlier arsenides, mainly along fractures and structural weaknesses. Its occurrence indicates a second hydrothermal pulse with distinct geochemical characteristics and possibly different fluid sources.

Geochemical analyses (this study; Meisser et al., 2012) confirm the dominance of a Co–Ni–As system, with strong positive correlations ($R^2 > 0.85$) among these elements. PCA analyses further distinguish an early arsenide phase from a later Cu–Mo–Au–Ag association. This trend supports a two-stage genetic model, with the primary mineralization associated with deep-seated, reduced fluids and the late-stage overprint related to more oxidized, possibly basinal or meteoric fluids. Gervilla et al. (2012) describe zoned chromite inclusions in arsenide minerals, confirming the genetic link between the ultramafic host and the ore. Maacha (2013) further highlighted the importance of the “Ambed crust” (silica–carbonate alteration zone), which caps the serpentinite and plays a crucial role in concentrating metals at structural-lithological boundaries.

Textural evidence, including brecciation, crack-seal textures, and rhythmic zoning in safflorite and skutterudite, reflects episodic fluid flow and fluctuating physicochemical conditions. The coexistence of idiomorphic and replacement textures suggests that mineralization occurred through both open-space filling and pervasive metasomatic alteration. Zoned chromite inclusions within arsenides, as described by Gervilla et al. (2012), confirm the genetic link between the ultramafic host and the ore minerals. The importance of the silica–carbonate alteration crust, or "Ambed" cap, overlying the serpentinite has also been emphasized by Maacha (2013) as a structural–lithological trap for ascending fluids. This cap, formed by hydrothermal alteration and near-surface weathering of ophiolitic rocks, played a crucial role in focusing mineral deposition along structural discontinuities (Fig. 8).

The genetic model of the Aghbar deposit, based on combined field, petrographic, structural, and geochemical evidence, highlights the role of a Pan-African ophiolitic host reworked by multiple

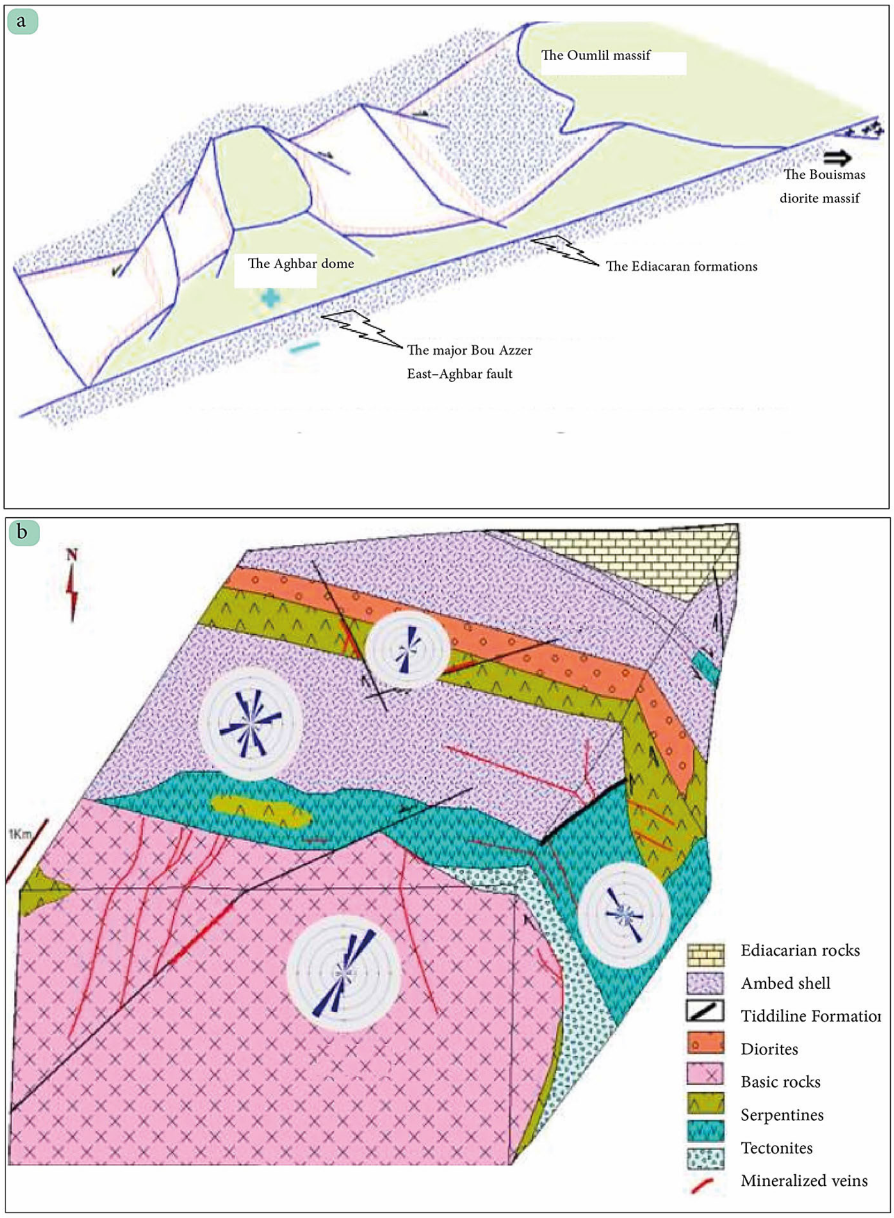

Figure 8. (a) Subsurface relationship between the Aghbar dome and the Oumlil massif (Maacha, 2013), (b) Synthetic model of the geological units, mineralized structures, and their distribution according to lithologies, proposed by Maacha (2013)

tectonic phases. Mineralization originated from a hybrid fluid system that evolved through three main stages. Initially, deep-seated, reducing fluids precipitated nickel- and cobalt-rich diarsenides and triarsenides in structurally prepared sites. These fluids were followed by cooler, Co–Fe–As-bearing solutions that replaced host serpentinites under metasomatic conditions. Lastly, a more oxidized fluid pulse introduced copper, molybdenum, and trace precious metals, overprinting and remobilizing the earlier assemblages (Fig. 8).

The resulting orebody is a vertically zoned, structurally guided system of veins and replacement bodies localized at lithological contacts and along NE-trending fault zones. This model is consistent with the framework proposed by Maacha (2013) and Gervilla et al. (2012), and displays parallels with other global cobalt districts, such as the Cobalt–Gowganda region in Canada. However, the distinct ophiolitic setting, serpentinized host rocks, and multiphase structural evolution confer a unique character to the Aghbar deposit. Understanding this model provides valuable guidance for exploration throughout the Bou Azzer district, especially in areas where serpentinite–volcanic interfaces are intersected by reactivated Pan-African faults.

CONCLUSIONS

The Aghbar deposit, located in the central part of the Bou Azzer–El Graâra inlier, represents a structurally complex and mineralogically diverse Co–Ni–As system hosted within a serpentinized ophiolitic sequence. The results of this multidisciplinary study confirm that the mineralization is the product of polyphase hydrothermal processes tightly controlled by structural and lithological factors.

Field observations and structural analysis demonstrate that mineralized quartz-carbonate veins are preferentially localized along major fault zones, particularly those trending ENE–WSW and NE–SW, which correspond to Pan-African and Hercynian tectonic reactivations respectively. The role of the serpentinite as both a mechanical and chemical trap is fundamental; its alteration into carbonated, brecciated, and silicified facies created favorable conditions for fluid-rock interaction and ore precipitation.

Petrographic and mineralogical observations reveal a multi-stage paragenesis evolving from early Ni-rich diarsenides to Co–Fe arsenides, and finally to late Cu-bearing sulfides and sulfosalts. The consistent association of chromite relicts within arsenide phases, and the textural evidence of replacement and zoning, support a dynamic fluid regime marked by episodic pulses and changing redox conditions.

Geochemical analyses reinforce this interpretation, highlighting a coherent Co–Ni–As signature across depth, supported by strong elemental correlations and PCA groupings. The superimposed Cu–Mo–Au–Ag association reflects a distinct, later hydrothermal event. These findings are consistent with previous works (e.g., Maacha, 2013; Gervilla et al., 2012), and confirm a two-stage metallogenic model: an early high-temperature arsenide-forming phase followed by a lower temperature sulfidic overprint.

This study contributes new evidence to support the model proposed by Maacha (2013) and refined by Tourneur (2019), in which the Aghbar-type mineralization reflects the interplay between a diapiric uplift of serpentinites, fault-controlled hydrothermal circulation, and localized metasomatic alteration. The genetic model for the Aghbar deposit thus highlights the importance of structural permeability, host-rock composition, and fluid evolution in shaping the mineral system.

These insights have important implications for ongoing exploration in the Bou Azzer district. Targeting serpentinite-volcanic contacts, ENE-trending faults, and zones of intense brecciation and carbonatization offers the best potential for discovering additional Co–Ni–As mineralization.

Acknowledgments

The authors sincerely thank the Managem Group for their valuable support during the fieldwork. Special thanks are extended to Mustapha Badri for preparing the thin sections used in this study.

REFERENCES

1. Admou, H., Razin, P., Egale, E., Youbi, N., Soulaimani, A., Blein, O., Chevremont, P., Gasquet, D., Barbanson, L., Bouabdelli, M., & Anzar, C. (2013). Notice explicative de la Carte géologiques du Maroc (1/50 000), feuille Aït Ahmane. *Notes et Mémoires du service Géologique du Maroc*, (533 bis), carte.
2. Aït Malek, H.A., Gasquet, D., Bertrand, J.M., Leterrier, J., 1998. Geochronologie U–Pb sur zircon de granitoïdes eburneens et panafricains dans

les boutonnières protérozoïques d'Igherm, du Kerdous et du Bas Draa (Anti-Atlas Occidental, Maroc). *C. R. Acad. Sci., Ser. II: Sci. Terre Planetes 327*(12), 819–826. https://doi.org/10.1016/s1251-8050(99)80056-1

3. Arenas, R., Martínez, S. S., Albert, R., Haissen, F., Fernández-Suárez, J., Pujol-Solà, N., ... & Gerdes, A. (2021). *100 myr cycles of oceanic lithosphere generation in peri-Gondwana: Neoproterozoic–Devonian ophiolites from the NW African–Iberian margin of Gondwana and the Variscan Orogen.* J. Geol. Soc. London, Spec. Publ. 503, SP503-2020–3. https://doi.org/10.1144/sp503-2020-3
4. Askkour, F., Ikenne, M., Chelle-Michou, C., Cousens, B. L., Markovic, S., Ousbih, M., ... & Ernst, R. (2024). Geochronology and petrogenesis of granitoids from the Bas Draa inlier (Western Anti-Atlas, Morocco): Revived debate on the tectonic regime operating during early Paleoproterozoic at the NW edge of the West African Craton. *Geochemistry, 84*(1), 126044. https://doi.org/10.1016/j.chemer.2023.126044
5. Baidada, B., Ikenne, M., Barbey, P., Soulaimani, A., Cousens, B., Haissen, F., ... & Alansari, A. (2019). SHRIMP U–Pb zircon geochronology of the granitoids of the Imiter Inlier: Constraints on the Pan-African events in the Saghro massif, Anti-Atlas (Morocco). *Journal of African Earth Sciences, 150*, 799–810. https://doi.org/10.1016/j.jafrearsci.2018.10.008
6. Barbey, P., Oberli, F., Burg, J.-P., Nachit, H., Pons, J., Meier, M. (2004). The Palaeoproterozoic in western Anti-Atlas (Morocco): a clarification. *J. Afr. Earth Sci. 39*, 39–245. https://doi.org/10.1016/j.jafrearsci.2004.07.044
7. Blein, O., Baudin, T., Chèvremont, P., Soulaimani, A., Admou, H., Gasquet, P., Cocherie, A., Egal, E., Youbi, N., Razin, P., Bouabdelli, M., Gombert, P. (2014a). Geochronological constraints on the polycyclic magmatism in the Bou Azzer-El Graara inlier (central anti-atlas Morocco). *J. Afr. Earth Sci. 99*, 287–306. https://doi. org/10.1016/j.jafrearsci.2014.04.021
8. Blein, O., Baudin, T., Soulaimani, A., Cocherie, A., Chèvremont, P., Admou, H., Ouanaimi, H., Hafi, A., Razin, P., Bouabdelli, M., Roger, J. (2014b). New geochemical, geochronological and structural constraints on the Ediacaran evolution of the south Sirwa, Agadir-Melloul and Iguerda inliers, Anti-Atlas, Morocco. *J. Afr. Earth Sci. 98*, 47–71. https://doi.org/10.1016/j.jafrearsci.2014.06.019
9. Bouabdellah, M., Maacha, L., Levresse, G., Saddiqi, O. (2016). *The Bou Azzer Co-Ni-Fe-As (±Au±Ag) district of central Anti-Antlas (Morocco): a long-lived late hercynian to triassic magmatic-hydrothermal to low-sulphidation epithermal system.* In: Mineral Deposits of North Africa. Springer International Publishing, 229–247. http://dx.doi.org/10.1007/978-3-319-31733-5_8
10. Bouougri, E. H., Ait Lahna, A., Tassinari, C.G., Basei, M., Youbi, N., Admou, H., Saquaque, A., Boumehdi, M. A., Maacha, L. (2020). Time constraints on Early Tonian Rifting and Cryogenian Arc terrane-continent convergence along the northern margin of the West African craton: Insights from SHRIMP and LA-ICP-MS zircon geochronology in the Pan-African Anti-Atlas belt (Morocco). Gondwana Research. https://doi. org/10.1016/j.gr.2020.03.011
11. Bouougri, E.H., Saquaque, A., (2004). Lithostratigraphic framework and correlation of the neoproterozoic northern western african craton passive margin sequence (Siroua Zenaga Bou Azzer-El Graara inliers, central anti-atlas, Morocco): an integrated approach. *J. Afr. Earth Sci. 39*, 227–238. https://doi.org/10.1016/j. jafrearsci.2004.07.045
12. Chevremont, Blein, O., Razin, P., Baudin, T., Barbanson, L., Gasquet, D., Soulaimani, A., Admou, H., Youbi, N., Bouabdelli, M., Anzar., C. (2013). Carte Géologique du Maroc au 1/50 000, feuille d'Ighriy. Notice explicative de la Carte géologiques du Maroc (1/50 000), feuille Bou Azer. *Notes et Mémoires du service Géologique du Maroc, 535* bis, pp.Carte. ⟨halsde-00950537⟩
13. Choubert, G. (1963). *Histoire géologique du précambrien de l'Anti-Atlas* [Doctoral Dissertation]. Éditions du Service géologique du Maroc.
14. D'Lemos, R.S., Inglis, J.D., Samson, S.D. (2006). A newly discovered orogenic event in Morocco: Neoproterozoic ages for supposed Eburnean basement of the Bou Azzer inlier, Anti-Atlas Mountains. *Precambrian Res. 147*, 65–78. https://doi.org/10.1016/j.precamres.2006.02.003
15. De Beer, C. H., Chevallier, L. P., De Kock, G. S., Gresse, P. G., & Thomas, R. J. (2000). Mémoire explicatif de la carte géologique du Maroc au 1/50 000, Feuille Sirwa. *Notes Mem. Serv. Geol. Maroc, 395*, 86.
16. Deynoux, M., Affaton, P., Trompette, R., & Villeneuve, M. (2006). Pan-African tectonic evolution and glacial events registered in Neoproterozoic to Cambrian cratonic and foreland basins of West Africa. *Journal of African Earth Sciences, 46*, 397–426. https://doi.org/10.1016/j.jafrearsci.2006.08.005
17. El Bahat, A., Ikenne, M., Soderlund, ¨ U., Cousens, B., Youbi, N., Ernst, R., Soulaimani, A., Janati, M., Ahmid Hafid, A. (2013). U–Pb baddeleyite ages and geochemistry of dolerite dykes in the Bas Dr aa inlier of the anti-atlas of Morocco: newly identified 1380 Ma event in the west african craton. *Lithos 174*, 85–98. https://doi.org/10.1016/j. lithos.2012.07.022
18. Gasquet, D., Ennih, N., Li´egeois, J.-P., Soulaimani, A., Michard, A. (2008). The PanAfrican belt. In:

Michard, A., Saddiqi, O., Chalouan, A., Frizon de Lamotte, D. (Eds.), *Continental Evolution: the Geology of Morocco. Lecture Notes in Earth Sciences*, 116. Springer-Verlag, Berlin Heidelberg, 33–64. https://doi.org/10.1007/978-3- 540-77076-3_2

19. Gervilla, F., Fanlo, I., Colás, V., & Subías, I. (2012). Mineral composition and phase relations of Ni–Co–Fe arsenide ores from the Aghbar mine, Bou Azzer, Morocco. *The Canadian Mineralogist, 50*, 447–470. https://doi.org/10.3749/canmin.50.2.447
20. Hefferan, K., Soulaimani, A., Samson, S. D., Admou, H., Inglis, J., Saquaque, A., Chaib, L., Heywood, N., (2014). A reconsideration of Pan African orogenic cycle in the Anti-Atlas Mountains, Morocco. *J. Afr. Earth Sci. 98*, 34–46. https://doi.org/10.1016/j. jafrearsci.2014.03.007
21. Hefferan, K., Admou, H., Karson, J. A., & Saquaque, A. (2000). Anti-Atlas (Morocco) role in Neoproterozoic Western Gondwana reconstruction. *Precambrian Research, 103*, 89–96. https://doi.org/10.1016/S0301-9268(00)00078-4
22. Hodel, F., Triantafyllou, A., Berger, J., Macouin, M., Baele, J.M., Mattielli, N., Monnier, C., Trindade, R.I.F., Ducea, M.N., Chatir, A., Ennih, N., Langlade, J., Poujol, M. (2020). The Moroccan Anti-Atlas ophiolites: timing and melting processes in an intra-oceanic arc-back-arc environment. *Gondwana Res. 86*, 182–202. https://doi.org/10.1016/j.gr.2020.05.014
23. Ikenne, M. Madi, A., Gasquet, D. Cheilletz, A. Hilal, R. Mortaji, A. Mhaili, E. (2005). Petrogenetic significance of podiform chromitites from the Neoproterozoic ophiolitic complex of Bou Azzer (Anti-Atlas, Morocco). *Africa Geoscience Review, 12*(2), 131–143.
24. Ikenne, M. Youbi, N. Ernst, R. Söderlund, U. Ait Lahna, A. Ousbih, M. Boumehdi M.A. Bekker, A. Bensalah, M.K. (2021). Discussion on “From Pan-African transpression to Cadomian transtension at the West African margin: New U-Pb zircon ages from the Eastern Saghro Inlier (Anti-Atlas, Morocco)” by Errami et al. 2020 (GSL-SP 503, 209-233). *Journal of the Geological Society*. https://doi.org/10.1144/jgs2020-206
25. Ikenne, M., Söderlund, U., Ernst, R. E., Pin, C., Youbi, N., Hafid, A. (2017). A c. 1710 Ma mafic sill emplaced into a quartzite and calcareous series from Ighrem, Anti-Atlas– Morocco: evidence that the Taghdout passive margin sedimentary group is nearly 1 Ga older than previously thought. *Journal of African Earth Sciences, 127*, 62–76. https://doi.org/10.1016/j.jafrearsci.2016.08.020
26. Ikenne, M., Souhassou, M., Cousens, B., Montero, P., Bea, F., Askkour, F., ... & Toummite, A. (2023). Zircon U–Pb geochronology and Sm–Nd and Rb–Sr isotope systematics of Neoproterozoic granitoïds from Bou Azzer (Anti-Atlas-Morocco): the obduction trigger of the central Anti-Atlas terrane. *Journal of African Earth Sciences, 202*, 104900. https://doi.org/10.1016/j.jafrearsci.2023.104900
27. Kouyaté, D., Soderlund, U., Youbi, N., Ernst, R., Hafid, A., Ikenne, M., Soulaimani, A., Bertrand, H., El Janati, M., Chaham, K.R. (2013). U–Pb baddeleyite and zircon ages of 2040 Ma, 1650 Ma and 885 Ma on dolerites in the west african craton (Anti-Atlas inlier): possible links to break-up of precambrian supercontinents. *Lithos 174*, 71–84. https://doi.org/10.1016/j.lithos.2012.04.028
28. Letsch, D., Large, S. J. E., Buechi, M. W., et al. (2018). Ediacaran glaciations of the West African Craton—Evidence from Morocco. *Precambrian Research*, *310*, 17–38. https://doi.org/10.1016/j.precamres.2018.02.015
29. Leblanc M. (1974). *Minéralisations cuprifères et volcanisme albitophyrique dans les ophiolites précambriennes de Bou Azzer* (Anti-Atlas, Maroc): Bull. Volc. 38, 1095–1109.
30. Leblanc, M. (1975). *Ophiolites précambriennes et gîtes arséniés de cobalt (Bou Azzer-Maroc)*. Unpublished Ph.D. thesis, Université de Paris VI, Paris, France, 367.
31. Leblanc, M., Lancelot, J.R. (1980). Interprétation géodynamique du domaine panafricain (Précambrien terminal) de l’Anti-Atlas (Maroc) à partir des données géologiques et géodynamiques. *Can. J. Earth Sci. 17*, 142–155. https://doi.org/10.1007/bf02597108
32. Leblanc, M. (1975). Ophiolites précambriennes et gites arseniés de cobalt: Bou Azzer (Maroc). These Doctorat d’Etat, Faculte des Science Paris VI, Memoires Centre Geologique et Geophysique.
33. Leblanc, M., and Arnold, M. (1994). Sulfur isotope evidence for the genesis of distinct mineralizations in the Bleida stratiform copper deposit (Morocco). *Econ. Geol. 89*, 931–935. https://doi.org/10.2113/gsecongeo.89.4.931
34. Maacha, L., Azizi, R., & Bouchta, R. (1998). Gisements cobaltifères du district de Bou Azzer (Anti-Atlas): structure, minéralogie et conditions de genèse. *Chronique de la recherche minière*, (531–532), 65–75.
35. Maacha, L. (2013). *Études métallogéniques et géophysiques des minéralisations cobaltifères et cuprifères de Bou-Azzer El Graara*, Anti-Atlas Maroc. Les minéralisations de cuivre de la plateforme de Bleida. Université Cadi Ayyad, Marrakech.
36. Maacha, L., El Ghorfi, M., Ennaciri, A., Sadiqqi, O., Soulaimani, A., Alansari, A., Bhilisse, M. (2015). Nouvelles données isotopiques et d’inclusions fluides des minéralisations cobaltifères de Bou Azzer: Apport à la géologie économique de la boutonnière (Anti-Atlas central, Maroc). *Notes et Mém.Serv.*

Géol. Maroc 579, 133–139.

37. Meisser, N., Gervilla, F., & Pinto, A. (2012). Supergene minerals from the Aghbar cobalt-nickel arsenide deposit, Bou Azzer, Morocco. *The Canadian Mineralogist, 50*, 471–485.
38. Naidoo, D.D., Bloomer, S.H., Saquaque, A., Hefferan, K., (1991). Geochemistry and significance of metavolcanic rocks from the Bou Azzer-El Graara ophiolite (Morocco). *Precambrian Res. 53*(1–2), 79–97. https://doi.org/10.1016/0301-9268(91)90006-v
39. O'Connor, E.A., Barnes, R.P., Beddoe Stephens, B., Fletcher, T., Gillespie, M.R., Hawkins, M.P., Loughlin, S.C., Smith, M., Smith, R.A., Waters, C.N., Williams, M., (2010). *Geology of the Drˆ aa, Kerdous, and Boumalne Districts, Anti Atlas, Morocco*. Nottingham British Geological Survey, Keyworth, 324.
40. Ousbih, M., Ikenne, M., Cousens, B., Chelle-Michou, C., El Bilali, H., Gaouzi, A., ... & Ernst, R. (2024). Stratigraphy, geochronology, geochemistry and Nd isotopes of the Ouarzazate Group, Anti-Atlas, Morocco: Evidence of a Late Neoproterozoic LIP in the northwestern part of the West African Craton. *Lithos, 474*, 107593. https://doi.org/10.1016/j.lithos.2024.107593
41. Salmi, S., Errami, E., Jouhari, A., El Kabouri, J., Ennih, N., Outaaoui, O., ... & Maacha, L. (2024). Constraints of the regional deformation on the hydrothermal veins in Ousdrat and Aït Ahmane ore deposits (Bou Azzer-El Graara inlier, central Anti-Atlas, Morocco): Implications for mineral exploration. *Journal of African Earth Sciences, 220*, 105441. https://doi.org/10.1016/j.jafrearsci.2024.105441
42. Saquaque, A., Admou, H., Karson, J., Hefferan, K., & Reuber, I. (1989). Precambrian accretionary tectonics in the Bou Azzer–El Graara region, Anti-Atlas, Morocco. *Geology, 17*, 1107–1110. https://doi.org/10.1130/0091-7613(1989)017
43. Soulaimani, A., Blein, O., Chèvremont, P., Ouanaimi, H., Hafid, A., Admou, H., ... & Beni Akhy, R. (2013). Notice explicative carte géol. Maroc (1/50 000), feuille Agadir Melloul. *Notes et Mémoires Serv. Géol. Maroc*, (549).
44. Toummite, A., Li´egeois, J.P., Gasquet, D., Bruguier, O., Beraaouz, E.H., Ikenne, M., 2013. Field, geochemistry and Sr-Nd isotopes of the pan-African granitoids from the Tifnoute Valley (Sirwa, anti-atlas, Morocco): a post-collisional event in a metacratonic setting. Mineral. *Petrol. 107*, 739–763. https://doi.org/10.1007/ s00710-012-0245-3
45. Tourneur, E., Chauvet, A., m Kouzmanov, K., Tuduri, J., Paquez, C., Sizaret, S., Darfal, A., Moundi, Y., El Hassani, A. (2021). Co-Ni-arsenide minealisation in the Bou-Azzer district (Anti-Atlas, Morocco): genetic model and tectonic implications. *Ore Geol. Rev. 134*, 1–25. https://doi.org/10.1016/j.oregeorev.2021.104128
46. Triantafyllou, A., Berger, J., Baele, J. M., Bruguier, O., Diot, H., Ennih, N., Monnier, C., Plissart, G., Vandycke, S., & Watlet, A. (2018). Intra-oceanic arc growth driven by magmatic and tectonic processes recorded in the Neoproterozoic Bougmane arc complex (Anti-Atlas, Morocco). *Precambrian Res. 304*, 39–63. https://doi.org/10.1016/j.precamres.2017.10.022
47. Tourneur, E. (2019). *Circulation de fluides aux abords de failles d'échelle crustale: contraintes structurales, microtectoniques, inclusions fluides et géochimiques sur les processus de formation du gisement de Bou Azzer (Ni-Co)*, Anti-Atlas, Maroc (Doctoral dissertation, Université Montpellier).
48. Villeneuve, M., & Cornée, J. J. (1994). Structure et évolution géodynamique de l'Anti-Atlas central (Maroc). *Bulletin de la Société Géologique de France, 165*, 247–258.
49. Walsh, G.J., Benziane, F., Aleinikoff, J.N., Harisson, R.W., Yazidi, A., Burton, W.C., Quick, J.E., Saadane, A., (2012). Neoproterozoic tectonic evolution of the Jebel Saghro and bou Azer-el Graara inliers, eastern and central anti-atlas, Morocco. *Precambrian Res*. 216–219, 23–62. https://doi.org/10.1016/j